Modeling the Interactions Among Neighboring Nanostructures for Local Feature Characterization and Defect Detection

Lijuan Xu and Qiang Huang, *Member, IEEE*

***Abstract*—Since properties of nanomaterials are determined by their structures, characterizing nanostructure feature variability and diagnosing structure defects are of great importance for quality control in scale-up nanomanufacturing. It is known that nanostructure interactions such as competing for source materials during growth contribute strongly to nanostructure uniformity and defect formation. However, there is a lack of rigorous formulation to describe nanostructure interactions and their effects on nanostructure variability. In this work, we develop a method to relate local nanostructure variability (quality measure) to nanostructure interactions under the framework of Gaussian Markov random field. With the developed modeling and estimation approaches, we are able to extract nanostructure interactions for any local region with or without defects based on its feature measurement. The established connection between nanostructure variability and interactions not only provides a metric for assessing nanostructure quality, but also enables a method to automatically detect defects and identify their patterns based on the underlying interaction patterns. Both simulation and real case studies are conducted to demonstrate the developed methods. The insights obtained from real case study agree with physical understanding.**

***Note to Practitioners*—Nanostructure features are often characterized by scanning electron microscope (SEM) or transmission electron microscope (TEM). Automatic assessment of nanostructure quality based on SEM or TEM images is essential for scale-up nanomanufacturing. We provide methods of automatic pattern extraction and defect detection to study nanostructure local variability.**

***Index Terms*—Defect detection, Gaussian Markov random field, local feature variability, nanostructure interaction.**

I. Introduction

LOW-DIMENSIONAL nanostructures such as carbon nanotubes and semiconductor nanowires are critical building blocks for nanodevices and nanosystems that have promising applications in fields like medicine and energy production [1]–[3]. For instance, high-density aligned nanotubes were fabricated to build submicron nanotube transistors with superior properties [4] and CMOS integrated circuits [5]. The improved performance is mainly due to the unique structures of nanomaterials. Taking Si nanowire solar cells as an example, efficiencies of light absorption and surface recombination can be greatly enhanced by the geometry and arrangement of nanowires [6]. On the other hand, nonuniformity and defects of nanostructures can cause performance degradation in nanodevices. For scale-up nanomanufacturing, it is therefore critical to develop metrics and methods to quantify nanostructure spatial variability or nonuniformity, and detect structure defects in each sample.

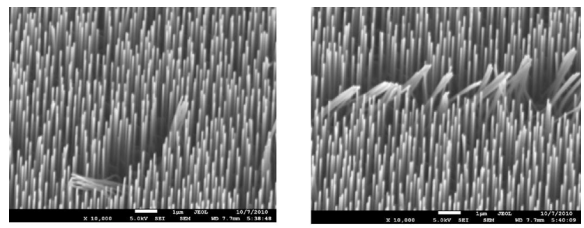

(a) (b)

Fig. 1. Samples of ZnO nanowires with (trend of) bundles, grown by VLS.

The formation of nanostructures and defects is sensitive to the interactions among neighboring structures such as competing for source materials during growth. Fig. 1 shows ZnO nanowires grown via VLS (vapor-liquid-solid) mechanism. Large nanowire bundles can inhibit the growth of neighboring nanowires by absorbing majority of Zn vapor [7]. Hence, improved understanding of nanostructure interactions will facilitate the control of local morphology and diagnosis of structure defects.

To control nanostructure synthesis variations and achieve scale-up nanomanufacturing, research has been conducted on nanowire growth process modeling [8]–[11], robust synthesis of nanostructures [12], [13], and nanoparticle dispersion quantification [14], [15]. The only work that quantifies the variability of continuous nanostructure features such as length is given by Huang [9]. Besides, only [9] and [14] have ever considered the interactions among nanostructures. Huang [9] attributed the local variability of nanowire length to the interacting effects among neighboring nanowires and [14] associated the clustering of nanoparticles to their interacting forces. But the interaction analysis was not the focus for either of the papers.

In this paper, we study the interactions among nanostructures in detail. For any local region of interest, we quantify the spatial

Manuscript received August 12, 2011; revised May 17, 2012; accepted June 22, 2012. Date of publication August 15, 2012; date of current version October 02, 2012. This paper was recommended for publication by Associate Editor P. Liu and Editor K. Bohringer upon evaluation of the reviewers' comments. This work was supported in part by the National Science Foundation under Grant CMMI-1000972.

The authors are with the Daniel J. Epstein Department of Industrial and Systems Engineering, University of Southern California, Los Angeles, CA 90089 USA (e-mail: qiang.huang@usc.edu).

Color versions of one or more of the figures in this paper are available online at http://ieeexplore.ieee.org.

Digital Object Identifier 10.1109/TASE.2012.2209417

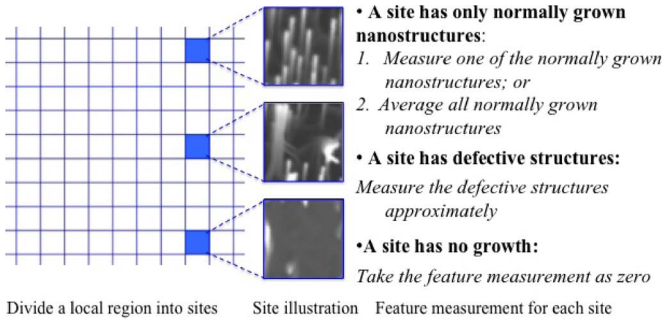

Fig. 2. Illustration of nanostructure feature measurement in a local region of interest.

variability of continuous quality features, e.g., length for nanostructures based on the extracted interaction patterns. With the established connection between nanostructure variability and nanostructure interactions, we can also detect the existence of defects within the region and identify detailed patterns for the defects.

Following this introduction, Section II introduces the problem formulation. Sections III and IV discuss the modeling and estimation of nanostructure interactions, respectively. Section V presents simulation case studies that demonstrate and validate our proposed strategies. Section VI provides a real case study for ZnO nanowires. At the end, Section VII will give a summary.

II. Problem Formulation

Our objective in this paper is to characterize nanostructure features in local regions of a substrate or "(nanostructure) local features" for short. Because of the important roles played by nanostructure interactions on local morphology, our characterization of local features will target on interaction patterns. Issues to be addressed include 1) modeling and estimating nanostructure interactions based on feature measurement and 2) quantifying local feature variability and identifying defects through interaction estimation.

We consider features in continuous scale like lengths of nanowires. With certain abstraction, nanostructures can be viewed to disperse in a real space with dimension 1, 2 or 3 depending on applications. We take a discrete sampling approach to measure nanostructures. Following steps are taken to measure nanostructure features in each local region of interest.

Step 1) We divide the local region regularly into non-overlapping sites (grids) as illustrated in Fig. 2. Denote the sites as $\boldsymbol{s} = \{\boldsymbol{s}_1, \boldsymbol{s}_2, \ldots, \boldsymbol{s}_n\}$.

Step 2) Measure and summarize nanostructures in site $\boldsymbol{s}_i$ as $X(\boldsymbol{s}_i)$. Altogether, we obtain a random field

$$\boldsymbol{X}(\boldsymbol{s}) = \{X(\boldsymbol{s}_1), X(\boldsymbol{s}_2), \ldots, X(\boldsymbol{s}_n)\}. \quad (1)$$

In detail, if a site has only normally grown nanostructures, we measure a randomly selected nanostructure or average all nanostructures in that site. Here, "normally grown" means the nanostructure is a single crystal and has no structural defects. If a site has defective structures, we measure the defective structures approximately by following the same procedure as that for normally grown nanostructures. And if there is no growth in the site, we take the feature measurement as zero for that site.

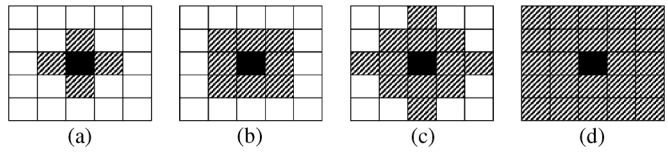

Fig. 3. Samples of candidate neighborhood structures: (a) first order (DS 1); (b) second order (SS 1); (c) DS 2; and (d) SS 2 (up diagonal filled grids are neighbors of the solid filled grid).

The grid size here establishes our sampling resolution and determines the length scale of corresponding interaction analysis. The length scale of interest will be determined by the structure property studied by nanoscientists. Our approach can be applied to any given scale.

Current techniques of measuring nanostructures are generally two dimensional imaging such as scanning electron microscopy (SEM) and transmission electron microscopy (TEM). Therefore, it is usually difficult to characterize defective structures due to their complex shapes. We suggest measuring these defects in the same way as measuring normally grown nanostructures. This approximation permits automatic measurement processing. At the same time, we can still identify defect patterns based on extracted interactions. This argument is validated in real case study of ZnO nanowire bundles. We provide a method to calculate nanowire lengths from SEM images in Appendix A.

Based on the feature measurement $\boldsymbol{X}(\boldsymbol{s})$, we model the feature field as a Gaussian Markov random field (GMRF) and estimate nanostructure interactions. More specifically, we will understand the interactions by finding for each site $\boldsymbol{s}_i$: 1) its neighbors, i.e. those sites that have interactions with $\boldsymbol{s}_i$ and 2) the relation between site $\boldsymbol{s}_i$ and its neighbors. Candidate neighborhood structures are illustrated in Fig. 3. They are of two forms: diamond schemes (DS) and square schemes (SS) of different orders. These two forms can cover most commonly observed interaction patterns.

We first model local features as stationary GMRF by assuming all nanostructures are normally grown. We then develop normality tests to detect defects. If there is no defect, the estimated stationary GMRF characterizes features' local variability. Otherwise, we relax the stationarity assumption and estimate interaction patterns for every site in the field individually. Defect patterns are then identified by "abnormally" strong interactions. Details are given in following sections.

III. Modeling of Nanostructure Interactions for Local Feature Characterization

We first decompose local nanostructure feature field $\boldsymbol{X}(\boldsymbol{s})$ into two parts: local trend or mean and local variability. Specifically, we take the following model

$$\boldsymbol{X}(\boldsymbol{s}) = \boldsymbol{Z}\boldsymbol{\gamma} + \boldsymbol{\Phi}(\boldsymbol{s}). \quad (2)$$

Here, $\boldsymbol{Z}\boldsymbol{\gamma}$ describes the local mean by a linear combination of explanatory variables Z that can be spatial location functions or concomitant data with each site [16]. $\boldsymbol{\Phi}(\boldsymbol{s})$ captures the local

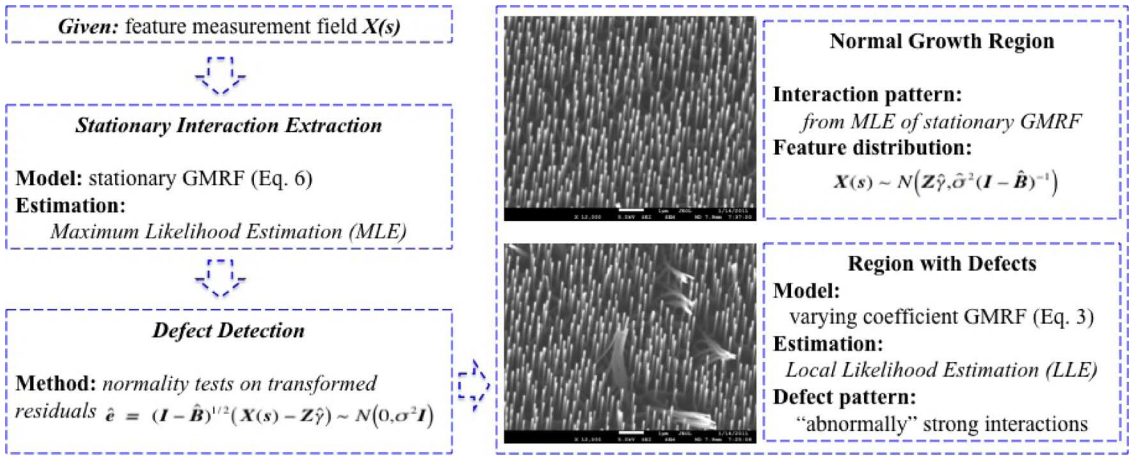

Fig. 4. Overall strategies of modeling and estimating nanostructure interactions for local feature characterization and automatic defect detection.

variability by describing interactions among neighboring nanostructures. This decomposition is different from Huang [9] because $\boldsymbol{Z\gamma}$ here extracts the *local* trend for the region of interest and is not characterized by growth kinetics.

We adopt Gaussian Markov random field (GMRF) [16], [17] to model nanostructure interactions and associate the interactions with local feature variability. Specifically, for each site $\boldsymbol{s}_i$, we define its neighbors and specify the conditional distribution of $\Phi(\boldsymbol{s}_i)$

$$\Phi(\boldsymbol{s}_i)|\left\{\phi(\boldsymbol{s}_j)\right\}_{j\neq i} \sim N\left(\sum_{\boldsymbol{s}_j\sim\boldsymbol{s}_i}\beta_{ij}\phi(\boldsymbol{s}_j),\sigma^2(\boldsymbol{s}_i)\right) \quad (3)$$

where $\boldsymbol{s}_j \sim \boldsymbol{s}_i$ means $\boldsymbol{s}_i$ and $\boldsymbol{s}_j$ are neighbors of each other, $\sigma^2(\boldsymbol{s}_i)$ is the conditional variance and β_{ij} is a spatial coefficient that is zero unless $\boldsymbol{s}_i \sim \boldsymbol{s}_j$. We interpret interactions among nanostructures as their mutual contributions on each other's local variability. Our modeling states, the conditional expectation of local feature variability in site $\boldsymbol{s}_i$ is a "weighted" sum of the local variabilities in its neighbors. Intuitively, the larger the "weights" (β_{ij}), the stronger the interactions.

GMRF has been extensively used in areas including spatial statistics [18], image analysis [19], [20] and disease mapping [21], etc. By varying the neighborhood structures and model parameters therein, GMRF is capable of modeling complex and diverse interaction structures. This property will certainly assist us to identify patterns of nanostructure interactions and develop a proper characterization of local features.

Denote $\boldsymbol{D} = \mathrm{diag}\{\sigma^2(\boldsymbol{s}_1),\ldots,\sigma^2(\boldsymbol{s}_n)\}$ and $\boldsymbol{B} = (\beta_{ij})$. From Brook's Lemma [22], when $(\boldsymbol{I}-\boldsymbol{B})$ is invertible and $(\boldsymbol{I}-\boldsymbol{B})^{-1}\boldsymbol{D}$ is symmetric and positive definite, $\boldsymbol{X}(\boldsymbol{s})$ follows a joint normal distribution as follows:

$$\boldsymbol{X}(\boldsymbol{s}) \sim N\left(\boldsymbol{Z\gamma},(\boldsymbol{I}-\boldsymbol{B})^{-1}\boldsymbol{D}\right) \quad (4)$$

which establishes the spatial distribution of nanostructure features. In particular, the covariance matrix $\boldsymbol{\Sigma} = (\boldsymbol{I}-\boldsymbol{B})^{-1}\boldsymbol{D}$ or equivalently the precision matrix $\boldsymbol{Q} = \boldsymbol{D}^{-1}(\boldsymbol{I}-\boldsymbol{B})$ clearly captures the local feature variability. Besides, it is easy to show the pairwise conditional correlation for any two sites $\boldsymbol{s}_i$ and $\boldsymbol{s}_j$ is [16]

$$\mathrm{corr}\left(X(\boldsymbol{s}_i),X(\boldsymbol{s}_j)|\left\{x(\boldsymbol{s}_k)\right\}_{k\neq i,j}\right) = \frac{\beta_{ij}}{|\beta_{ij}|}\sqrt{\beta_{ij}\beta_{ji}}. \quad (5)$$

Quantitatively, the stronger the conditional correlations, the stronger the interactions among neighboring nanostructures.

For a local region that has no defect (i.e., normal/uniform growth of nanostructures), we may assume stationary interaction patterns for every site across the field. That is $\sigma^2(\boldsymbol{s}_i) = \sigma^2$ and $\beta_{ij} = \beta_{\boldsymbol{q}}$ where $\boldsymbol{q} = \boldsymbol{s}_i - \boldsymbol{s}_j$. The conditional characteristics are thus

$$\Phi(\boldsymbol{s}_i)|\left\{\phi(\boldsymbol{s}_j)\right\}_{j\neq i} \sim N\left(\sum_{\boldsymbol{s}_j\sim\boldsymbol{s}_i}\beta_{\boldsymbol{q}}\phi(\boldsymbol{s}_j),\sigma^2\right) \quad (6)$$

for any site $\boldsymbol{s}_i$. Due to symmetry of the precision matrix, we have $\beta_{ij} = \beta_{ji}\ \forall i,j$ and $\beta_{\boldsymbol{q}} = \beta_{-\boldsymbol{q}}$ for any $\boldsymbol{q} > \boldsymbol{0}$. Besides, $\mathrm{corr}(X(\boldsymbol{s}_i),X(\boldsymbol{s}_j)|\{x(\boldsymbol{s}_k)\}_{k\neq i,j}) = \beta_{\boldsymbol{q}}$. $\beta_{\boldsymbol{q}}$ directly explains interactions between site $\boldsymbol{s}_i$ and site $\boldsymbol{s}_j$.

We call the modeling in (6) with stationarity assumptions "stationary GMRF modeling." Correspondingly, GMRF of general forms in (3) is called "nonstationary" or "varying coefficient GMRF." Because nonstationary GMRF involves much more unknown parameters, for model parsimony we always try stationary GMRF modeling first. Only for local regions that have been detected to have defects, we then turn to nonstationary GMRF to identify the detailed defect patterns.

IV. Estimation of Nanostructure Interactions for Local Feature Characterization

As introduced in Section III, we model nanostructure interactions in terms of conditional correlations between sites. Under the framework of GMRF, nanostructure interactions and local features are described by model parameters $\boldsymbol{\eta} = \{\beta_{ij},\sigma^2(\boldsymbol{s}_i),\boldsymbol{\gamma}\}_{i,j=1,\ldots,n}$ in (4). Due to the computation of matrix determinant $|\boldsymbol{I}-\boldsymbol{B}|$, maximum-likelihood estimation (MLE) approach is only feasible for stationary GMRF defined on regular fields. Therefore, we follow strategies in Fig. 4 to estimate nanostructure interactions. Particularly, we apply MLE to estimate stationary interactions in normal growth regions and local likelihood estimation (LLE) to estimate nonstationary interactions in regions with defects. Normality tests on transformed residuals detect defects initially based on stationary interaction estimation.

A. Maximum-Likelihood Estimation (MLE) for Stationary Nanostructure Interactions

If nanostructure interactions are modeled by stationary GMRF, the local features follow a normal distribution $N(\boldsymbol{Z\gamma}, \sigma^2(\boldsymbol{I}-\boldsymbol{B})^{-1})$. Since we divide regions of interest regularly, $\boldsymbol{I}-\boldsymbol{B}$ is a block circulant matrix under periodic boundary conditions. We can thus efficiently calculate $|\boldsymbol{I}-\boldsymbol{B}|$ through Fast Fourier Transformation (FFT). Consequently, MLE is feasible and efficient in this case.

We summarize the MLE approach as follows by referring to relevant literatures [16], [17], [23]–[26]. First, we can write the negative log likelihood as

$$\begin{aligned} 2L(\boldsymbol{\eta}|\boldsymbol{x}(\boldsymbol{s})) &= -2\log f(\boldsymbol{x}(\boldsymbol{s})|\boldsymbol{\eta}) \\ &= \frac{1}{\sigma^2}(\boldsymbol{x}(\boldsymbol{s})-\boldsymbol{Z\gamma})^T(\boldsymbol{I}-\boldsymbol{B})(\boldsymbol{x}(\boldsymbol{s})-\boldsymbol{Z\gamma}) \\ &\quad + n\log\sigma^2 - \log(|\boldsymbol{I}-\boldsymbol{B}|) + c \end{aligned} \tag{7}$$

where $\boldsymbol{\eta} = \{\beta_{\boldsymbol{q}}, \sigma^2, \boldsymbol{\gamma}\}_{\boldsymbol{q}>\boldsymbol{0}}$ denotes the collection of unknown parameters, n is the total number of random variables (sites) in the field and c is a known constant. Let $\hat{\boldsymbol{\eta}} = \{\hat{\beta}_{\boldsymbol{q}}, \hat{\sigma}^2, \hat{\boldsymbol{\gamma}}\}$ be the MLE of $\boldsymbol{\eta}$. Then, setting $\partial L/\partial\sigma^2 = 0$, we obtain

$$\hat{\sigma}^2 = n^{-1}(\boldsymbol{x}(\boldsymbol{s})-\boldsymbol{Z\gamma})^T(\boldsymbol{I}-\boldsymbol{B})(\boldsymbol{x}(\boldsymbol{s})-\boldsymbol{Z\gamma}). \tag{8}$$

Similarly setting $\partial L/\partial\boldsymbol{\gamma} = \boldsymbol{0}$, we can see $\hat{\boldsymbol{\gamma}}$ is the generalized LSE for linear regression: $\boldsymbol{x}(\boldsymbol{s}) = \boldsymbol{Z\gamma} + \boldsymbol{\epsilon}$ with $\boldsymbol{\epsilon} \sim MVN(\boldsymbol{0}, (\boldsymbol{I}-\boldsymbol{B})^{-1})$, or equivalently

$$\hat{\boldsymbol{\gamma}} = \left(\boldsymbol{Z}^T(\boldsymbol{I}-\boldsymbol{B})\boldsymbol{Z}\right)^{-1}\boldsymbol{Z}^T(\boldsymbol{I}-\boldsymbol{B})\boldsymbol{x}(\boldsymbol{s}). \tag{9}$$

Therefore, $\hat{\boldsymbol{\beta}} = \arg\min \mathfrak{L}(\boldsymbol{\beta}|\boldsymbol{x}(\boldsymbol{s}))$ with $\boldsymbol{\beta} = \{\beta_{\boldsymbol{q}}\}_{\boldsymbol{q}>\boldsymbol{0}}$ and

$$\begin{aligned} \mathfrak{L}(\boldsymbol{\beta}|\boldsymbol{x}(\boldsymbol{s})) = \log\left\{(\boldsymbol{x}(\boldsymbol{s})-\boldsymbol{Z\hat{\gamma}})^T(\boldsymbol{I}-\boldsymbol{B})(\boldsymbol{x}(\boldsymbol{s})-\boldsymbol{Z\hat{\gamma}})\right\} \\ -n^{-1}\log(|\boldsymbol{I}-\boldsymbol{B}|). \end{aligned} \tag{10}$$

Based on $\hat{\boldsymbol{\beta}}$, we can obtain $\hat{\sigma}^2$ and $\hat{\boldsymbol{\gamma}}$ from (8) and (9). In addition, if we denote τ^2 as the unconditional variance for $X(\boldsymbol{s}_i), \forall i$, then $\hat{\tau}^2 = \hat{\sigma}^2(\boldsymbol{I}-\hat{\boldsymbol{B}})^{-1}_{11}$ ((4)).

$\hat{\boldsymbol{\eta}}$ is a consistent estimator of $\boldsymbol{\eta}$ for stationary GMRF. Besides, $\hat{\boldsymbol{\eta}}$ follows a joint normal distribution with mean $\boldsymbol{\eta}$ and precision matrix $\boldsymbol{J}(\boldsymbol{\eta})$ (the fisher information matrix) asymptotically [16], [27]. Confidence intervals/elipsoid for $\hat{\boldsymbol{\eta}}$ can be obtained accordingly. Models of different neighborhood structures can also be compared through asymptotic likelihood ratio tests (LRT) [23]. GMRF with the winning neighborhood structure will be selected to describe the stationary interactions.

Estimation of stationary nanostructure interactions can be viewed as an overall estimation of interactions for the local region. We use it as a benchmark to detect defects. For normal growth regions, it also specifies the spatial distribution of nanostructure features: $N(\boldsymbol{Z\hat{\gamma}}, \hat{\sigma}^2(\boldsymbol{I}-\hat{\boldsymbol{B}})^{-1})$ and determines the interaction patterns for each site.

B. Normality Tests on Transformed Residuals to Detect Defects

Since normally grown nanostructures have stationary interaction patterns across sites, deviation of our measurement data from the stationary interaction pattern indicates potential defects. Therefore, we can formulate the defect detection problem as a problem of testing the following hypotheses.

H_0 Measured nanostructure feature field follows stationary GMRF.

H_1 Measured nanostructure feature field follows nonstationary GMRF.

We define the transformed residuals as

$$\boldsymbol{e} = (\boldsymbol{I}-\boldsymbol{B})^{\frac{1}{2}}(\boldsymbol{X}(\boldsymbol{s})-\boldsymbol{Z\gamma}). \tag{11}$$

Under the null hypothesis H_0, we have $\boldsymbol{X}(\boldsymbol{s}) \sim N(\boldsymbol{Z\gamma}, \sigma^2(\boldsymbol{I}-\boldsymbol{B})^{-1})$ by referring to (4) and (6). Therefore, the transformed residuals $\boldsymbol{e} \sim N(0, \sigma^2\boldsymbol{I})$. Based on stationary GMRF estimation, we obtain MLEs of transformed residuals as

$$\hat{\boldsymbol{e}} = (\boldsymbol{I}-\hat{\boldsymbol{B}})^{\frac{1}{2}}(\boldsymbol{X}(\boldsymbol{s})-\boldsymbol{Z\hat{\gamma}}). \tag{12}$$

Taking into account the consistency property of $\hat{\boldsymbol{\eta}} = \{\hat{\beta}_{\boldsymbol{q}}, \hat{\sigma}^2, \hat{\boldsymbol{\gamma}}\}_{\boldsymbol{q}>0}$, MLEs of transformed residuals $\hat{e}_i, i = 1, \ldots, n$ are also i.i.d. normal random variables asymptotically. That is

$$\hat{e}_i \sim \text{i.i.d. } N(0, \sigma^2) \text{ for } i = 1, \ldots, n \tag{13}$$

asymptotically if stationary GMRF really captures the interaction patterns among measurement data. On the contrary, if there are some defects, due to the inaccurate interaction extraction for defective sites, transformed residuals of defective sites would be larger comparing to those of normal sites. Therefore, evaluating the deviation of $\hat{e}_i, i = 1, \ldots, n$ from i.i.d. normal distributions will help detecting defects.

We perform normality tests on transformed residuals $\hat{\boldsymbol{e}}$ to detect defects. Normality tests detect "outliers" among $\hat{e}_i$, $i = 1, \ldots, n$. Comparing to other tests e.g. χ^2 test which test on the equal variance assumption, normality tests are more powerful defect detection method when the percentage of defects is small. Both graphical methods including normality plots and formal tests including the Anderson-Darling test, the Cramervon-Mises test, and the Lilliefors test, etc., can be used. Thode [28] has a good summary of normality test methods. In this paper, we recommend half-normal plot for visual judgment because it has a clearest indication of outliers. Anderson-Darling test is chosen for formal detection because its calculation on departure of empirical distributions from normality puts more weights on tails [29] and thus it is more sensitive to defects.

If normality tests indicate the existence of defects in our measurement data, the LLE technique is then used to estimate interactions across the field. Patterns of defects will be identified by patterns of interactions.

C. Local Likelihood Estimation (LLE) for Regions With Defects

For regions detected to have defects, we use varying coefficient GMRF to model the nonstationary interactions among nanostructures. Since spatial parameters $\{\beta_{ij}\}_{i=1,\ldots,n,\boldsymbol{s}_j\sim\boldsymbol{s}_i}$ vary across sites, dimension of unknown parameters is larger than measurement data. Traditional estimation methods (e.g.,

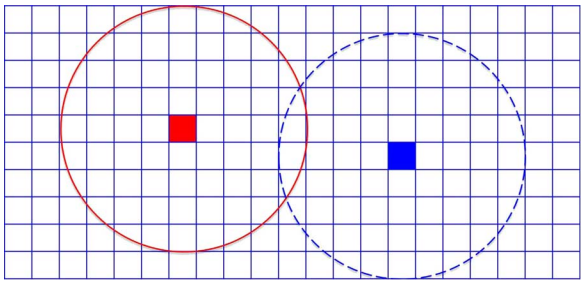

Fig. 5. Illustration of LLE.

MLE, pseudo-likelihood, coding method, etc., [16], [17], and [25]) are not directly applicable here.

We adopt LLE to estimate nanostructure interactions. Parameters $\{\beta_{ij}\}_{\boldsymbol{s}_j\sim\boldsymbol{s}_i}$ and $\sigma^2(\boldsymbol{s}_i)$ that define the interactions of any site $\boldsymbol{s}_i$ with its neighbors are estimated based on those sites physically near $\boldsymbol{s}_i$. As illustrated in Fig. 5, given window size $\lambda = 4$ we use sites within the corresponding circles to estimate the interactions for colored target sites. Denote $\boldsymbol{R}^\lambda(\boldsymbol{s}_i)$ (including $\boldsymbol{s}_i$) to be the collection of sites included for estimating $\boldsymbol{s}_i$ under λ. To estimate parameters $\{\beta_{ij}\}_{\boldsymbol{s}_j\sim\boldsymbol{s}_i}$ and $\sigma^2(\boldsymbol{s}_i)$, we assume stationary interaction patterns among $\boldsymbol{R}^\lambda(\boldsymbol{s}_i)$. In addition, we assign different weight $W_k^\lambda(\boldsymbol{s}_i)$ to each site $\boldsymbol{s}_k \in \boldsymbol{R}^\lambda(\boldsymbol{s}_i)$. The weight $W_k^\lambda(\boldsymbol{s}_i)$ measures how much we believe the interaction pattern of $\boldsymbol{s}_k$ is close to that of $\boldsymbol{s}_i$.

For each site $\boldsymbol{s}_i$, pseudo likelihood is chosen to estimate its parameters because of the total computation complexity. In this way, $\{\beta_{ij}, \sigma^2(\boldsymbol{s}_i)\}_{\boldsymbol{s}_j\sim\boldsymbol{s}_i}$ is the weighted least squares estimator for linear regression

$$X(\boldsymbol{s}_k) = \beta_{i0} + \sum_{\boldsymbol{s}_j\sim\boldsymbol{s}_i} \beta_{ij} X(\boldsymbol{s}_k + \boldsymbol{s}_j - \boldsymbol{s}_i) + \epsilon_{ik} \tag{14}$$

where $\boldsymbol{s}_k \in \boldsymbol{R}^\lambda(\boldsymbol{s}_i)$ for any $i = 1, \ldots, n$ under given λ. Here, β_{i0} is the intercept and ϵ_{ik} is the kth error term. We select the smoothing parameter λ (i.e. the window size) by cross validations [30]. Bias correction on raw estimation of $\{\beta_{ij}\}_{i=1,\ldots,n,\boldsymbol{s}_j\sim\boldsymbol{s}_i}$ from (14) is then performed by referring to (15) in [31]. Interested readers please refer to [31], [32], and references therein for more details.

V. Simulation Case Studies

Simulation case studies are to illustrate and validate our proposed modeling and estimation procedures for extracting nanostructure interactions and characterizing nanostructure local features.

A. Setups of Simulation Experiments

We simulated 100 i.i.d. datasets defined on 50×100 regular lattice $\boldsymbol{s} = \{(s,t)\}_{s=1,\ldots,50,t=1,\ldots,100}$. These datasets mimic (replicates of) feature measurement fields we may obtain from normal growth regions. Each dataset has structure $\boldsymbol{X}(\boldsymbol{s}) = \boldsymbol{Z}\boldsymbol{\gamma} + \boldsymbol{\Phi}(\boldsymbol{s})$ as in (2). The local trend $\mathbb{E}\boldsymbol{X}(\boldsymbol{s}) = \boldsymbol{Z}\boldsymbol{\gamma}$ is defined as

$$\mathbb{E}X(s,t) = \gamma_0 + \gamma_1 * s + \gamma_2 * t. \tag{15}$$

TABLE I
Parameter Values Set in Simulation Studies

γ_0	γ_1	γ_2	β_1	β_2	β_3	β_4	σ^2
6.00	-0.03	-0.01	-0.1	0.25	0.05	0.15	1

TABLE II
Summary of MLEs for $\boldsymbol{\gamma}$, $\boldsymbol{\beta}$ and σ^2 Based on Stationary Datasets (95 Samples)

	True Val.	Est. Mean	Std. Dev.	5% Qt.	95% Qt.
γ_0	6.00	6.0020	0.0744	5.8740	6.1113
γ_1	-0.03	-0.0299	0.0016	-0.0328	-0.0276
γ_2	-0.01	-0.0101	0.0009	-0.0116	-0.0087
β_1	-0.10	-0.1013	0.0131	-0.1246	-0.0825
β_2	0.25	0.2512	0.0102	0.2324	0.2660
β_3	0.05	0.0477	0.0101	0.0333	0.0626
β_4	0.15	0.1506	0.0140	0.1300	0.1756
σ^2	1.00	0.9958	0.0219	0.9636	1.0355

The nanostructure interaction field $\boldsymbol{\Phi}(\boldsymbol{s})$ follows stationary GMRF with second-order neighborhood structure. That is, for each site $\boldsymbol{s}_i = (s,t) \in \boldsymbol{s}$, we have

$$\begin{aligned}\mathbb{E}\Phi(s,t)|\{\phi(s',t')\}_{(s',t')\neq(s,t)} &= \beta_1\{\phi(s-1,t-1)+\phi(s+1,t+1)\}\\ &+ \beta_2\{\phi(s-1,t)+\phi(s+1,t)\}\\ &+ \beta_3\{\phi(s-1,t+1)+\phi(s+1,t-1)\}\\ &+ \beta_4\{\phi(s,t-1)+\phi(s,t+1)\}\end{aligned} \tag{16}$$

and $\mathrm{Var}(\Phi(s,t)|\{\phi(s',t')\}_{(s',t')\neq(s,t)} = \sigma^2$. Values set for simulating the datasets are summarized in Table I. We include both positive and negative values for $\boldsymbol{\beta}$ to explore the most general patterns of nanostructure interactions.

B. Interaction Extraction for Normal Growth Regions

For each previously simulated dataset (referred as *stationary datasets*), we model it as stationary GMRF with local trend $\mathbb{E}X(s,t) = \gamma_0 + \gamma_1 * s + \gamma_2 * t$. We then estimate parameters and interaction schemes for GMRF models by MLE.

Different neighborhood structures are compared based on asymptotic likelihood ratio tests [23] at 95% confidence level. Among the 100 datasets, 95 datasets correctly select second-order scheme to describe the interaction structure, while the other five datasets select diamond scheme (DS 2 in Fig. 3).

As to parameter estimation, we summarize MLEs of $\boldsymbol{\gamma}$, $\boldsymbol{\beta}$, and σ^2 in Table II based on those 95 datasets that select second order scheme. From the results we can see MLEs of parameters are quite stable among different datasets and are very close to their corresponding true values. We also plot MLEs of β_i, $i = 1, \ldots, 4$ together with their 95% confidence bounds in Fig. 6. Vibrations of confidence bounds are due to the randomness among different datasets (i.i.d. samples from the same distribution). From the figure, we can see the 95% confidence intervals of β_i, $i = 1, \ldots, 4$ contain corresponding true values almost all times.

Although we know there is no defect in our simulated data, we still do normality tests to detect defects as described in Section IV. Among the 100 simulated datasets, 97 of them have an Anderson-Darling p value greater than 5%. That is at 95%

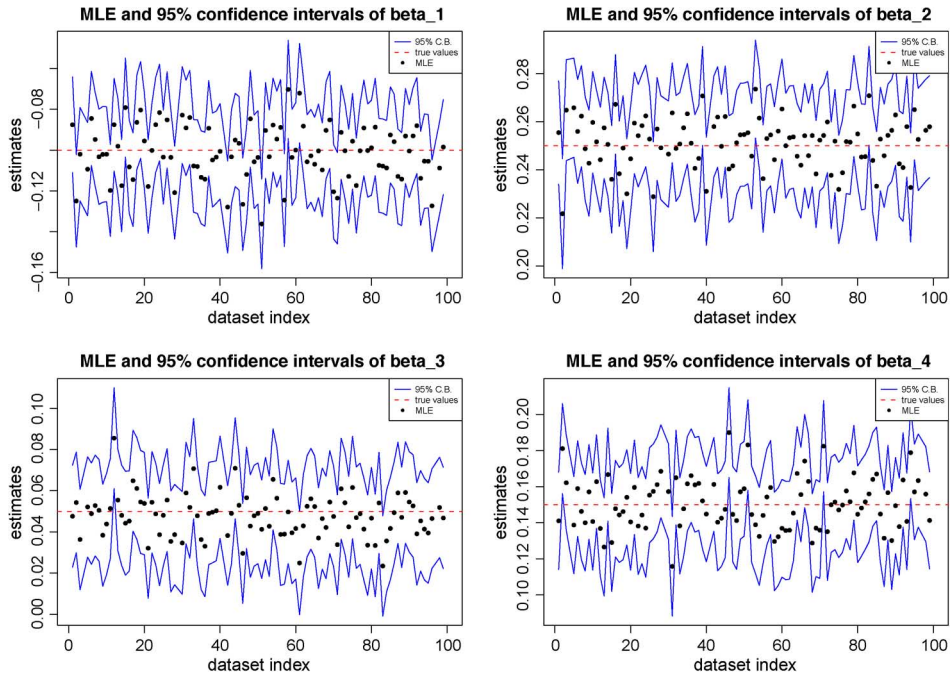

Fig. 6. MLEs and 95% confidence bounds of β_i, $i = 1, \ldots, 4$.

confidence level only 3 out of 100 datasets are falsely detected to have defects. Our method for detecting defects works well for normal growth regions.

The simulation study of stationary datasets shows our method can correctly extract interaction patterns for normal growth regions. The estimated stationary GMRF accurately describes features' spatial variability. We also have high confidence that our suggested normality tests do not falsely indicate defects.

C. Interaction Extraction for Defects Detection

For each stationary dataset, we set randomly 50–250 sites in it as zeros (i.e., 1%–5% zero ratio). They mimic those no growth sites caused by underlying deformities of the substrate. By studying these *nonstationary datasets*, we hope our estimation of nanostructure interactions and proposed normality tests can detect them and identify their patterns.

Following the strategies summarized in Fig. 4, we first model each nonstationary dataset through stationary GMRF pretending all nanostructures are normally grown. Then, normality tests are performed to detect defects based on MLEs of the transformed residuals $(\boldsymbol{I} - \hat{\boldsymbol{B}})^{1/2}(\boldsymbol{x}(\boldsymbol{s}) - \boldsymbol{Z}\hat{\boldsymbol{\gamma}})$. For the 100 nonstationary datasets, Anderson-Darling p values are all nearly zero $(< 10^{-32})$ indicating the existence of defects in all datasets. Our defect detection result here is 100% consistent with reality.

We then randomly select one dataset to illustrate the identification of detailed defect patterns by nonstationary interaction estimation. We model the selected dataset by varying coefficient GMRF (3) with second order neighborhood structure based on its overall interaction estimation. We then estimate the interactions by local likelihood technique under $\lambda = 12$ (Fig. 7). Level plots of estimated β_i, $i = 1, \ldots, 4$ are in Fig. 8. We also add

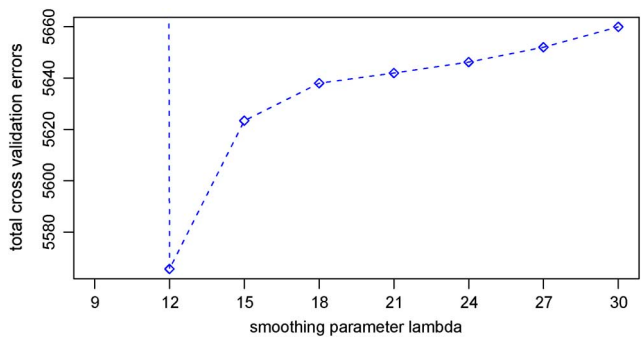

Fig. 7. λ selection by cross validation [32] simulation study.

locations of designed no growth sites to assist visual comparison. Here, β_i, $\forall i$ has the same meaning as that explained in simulation setups. Therefore, values of β_i, $\forall i$ determine the intensity of interactions across the field. Directions of the interactions are indicated by corresponding red arrows beside the level plots. From the figure, we can see local peaks of nanostructure interactions are always related to those no growth sites. This observation is both consistent with the data: higher correlation between zeros and their neighboring values and the physics: defects have higher impact on neighboring sites due to competition of source materials, etc.

To summarize the simulation studies presented above, our proposed strategies to characterize local features and detect defects by extracting nanostructure interactions are feasible and effective. Although no growth may be an extreme form of "defects," our results suggest that it is feasible in general cases to identify defects by extracting interaction patterns from feature measurement. The real case study of large bundle defects supports this claim in the following section.

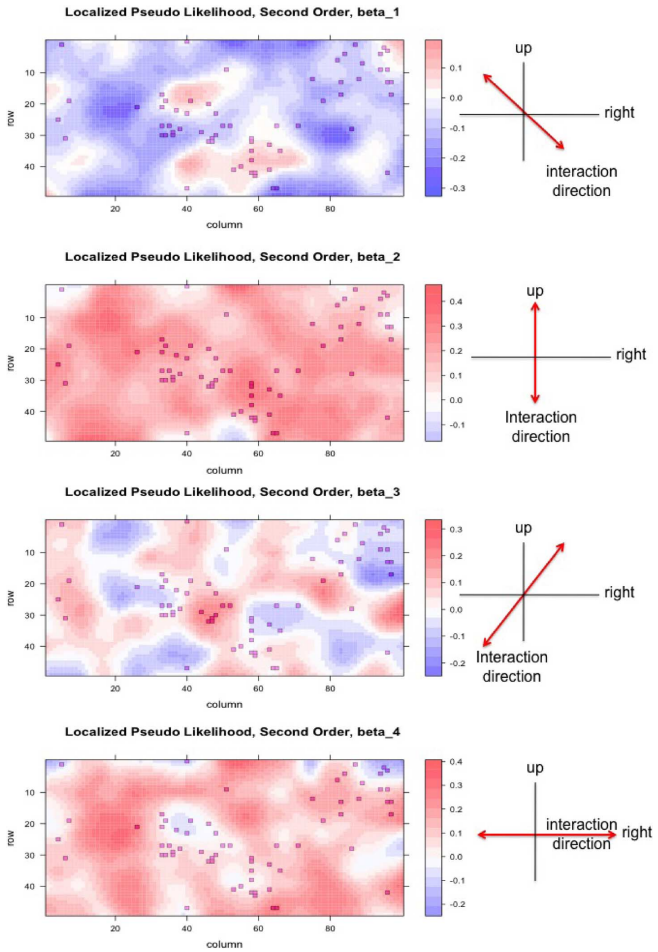

Fig. 8. Level plots of local likelihood estimated $\boldsymbol{\beta}$ together with simulated no growth sites.

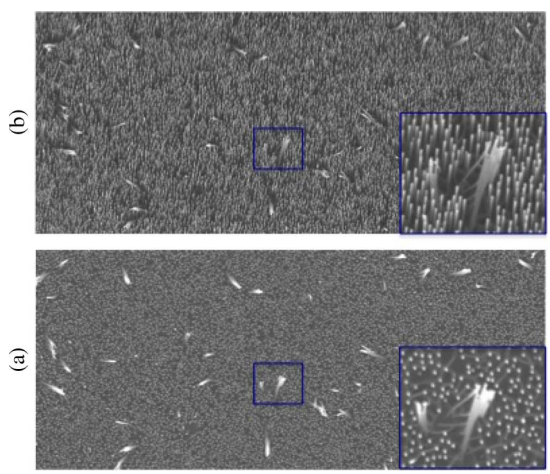

Fig. 9. SEM images of ZnO nanowire sample. Insets are enlarged images for the labeled area.

VI. Real Case Study: ZnO Nanowire Experiment Data Analysis

In this section, we are going to study interactions among nanowires through length measurement to automatically detect nanowire bundles (insets of Fig. 9).

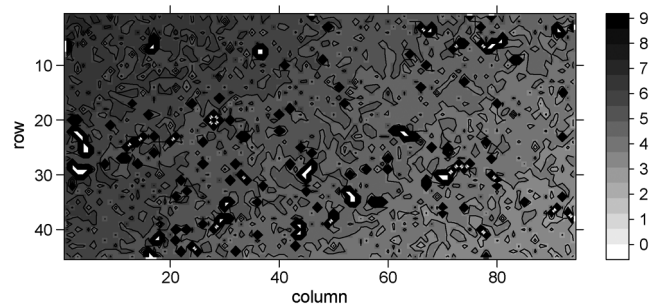

Fig. 10. Level plot of nanowire length field.

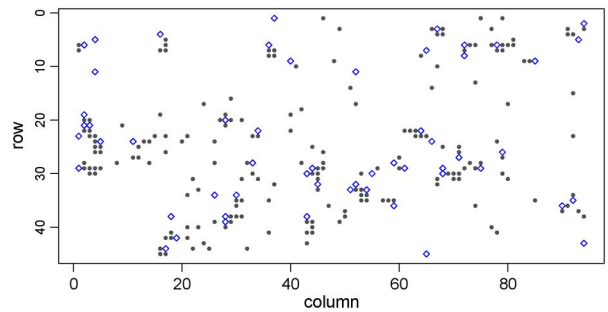

Fig. 11. Locations of NW bundles ($\diamond$) and no growth sites ($\bullet$).

We measured a 27 um $\times$ 56.4 um local region of a ZnO nanowire sample which was grown through VLS at 950 °C, 1 atm. with 100 sccm Ar. flow for 25 min. Two SEM images are taken for the same region with one from the top and the other by tilting the sample for 8° (as shown in Fig. 9). By extracting tip locations of the same nanowire on the two images, we can calculate the length of the nanowire. Please refer to Appendix A for more details.

We then divide the region regularly into 45 $\times$ 94 grids (sites) each of size 0.6 um $\times$ 0.6 um. For each site, we measure a randomly selected nanowire if there is. If a site has no growth, we take the length measurement as zero. And if a site is occupied by a nanowire bundle, we measure the bundle approximately as measuring straight nanowires. Altogether, we obtain a 45 $\times$ 94 nanowire length field.

A. Preliminary Data Analysis

We first look at the data graphically. Figs. 10 and 11 show a level plot of the NW length field (with contour lines) and locations of nanowire bundles and no growth sites, respectively. From the figure, we can see: 1) neglecting no growth sites, nanowire lengths generally decrease from top to bottom and from left to right and 2) nanowire bundles are normally surrounded by no growth sites indicating stronger impact of bundles on their neighboring sites.

We further plot nanowire lengths with corresponding row and column indexes of the field in Fig. 12. Those no growth sites are neglected to give a clearer view of the trend. Lengths of nanowire bundles (approximate) are indicated by blue diamonds. Our findings are: 1) local trend of the lengths is generally linear with row and column indexes and 2) nanowire bundles cannot be identified directly by their lengths.

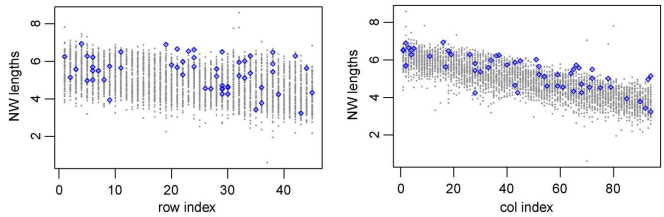

Fig. 12. NW lengths versus row indexes and column indexes of the measured field.

TABLE III
MLEs AND 95% C.I.S OF STATIONARY GMRF PARAMETERS FOR NW LENGTH FIELD

γ_1	γ_2	γ_3	σ^2
6.5648 (6.424, 6.706)	-0.0295 (-0.034,-0.026)	-0.0254 (-0.027, -0.023)	1.0865 (1.039,1.134)
β_1	β_2	β_3	β_4
0.0605 (0.032, 0.089)	0.0810 (0.051, 0.111)	0.0585 (0.030, 0.087)	0.1384 (0.110,0.167)

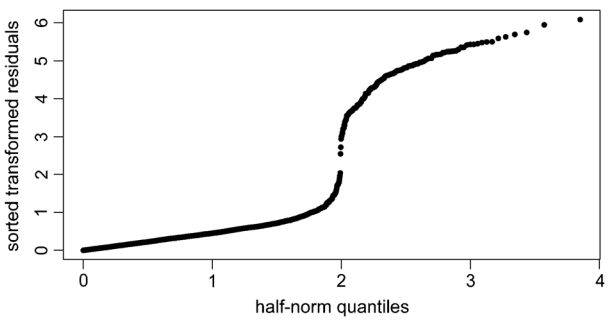

Fig. 13. Half-normal plot for transformed residuals $\hat{\boldsymbol{e}}$, real case study.

Therefore, we propose to detect bundles by extracting interaction patterns. Besides, we take the local trend as $\mathbb{E}X(s,t) = \gamma_0 + \gamma_1 * s + \gamma_2 * t$ [same as (15)] with $\boldsymbol{s} = \{(s,t)\}_{s=1,2,\ldots,45, t=1,2,\ldots,94}$ in stationary GMRF modeling at first step.

B. Interaction Extraction for NW Bundle Detection

We first model the length field as a stationary GMRF with its local trend as in (15) pretending we do not know there are defects within the field. Our motivations are: 1) to get an overall estimate of local trend and nanowire interactions and 2) to check whether our method can automatically detect defects without looking at the images.

By stationary GMRF modeling, we select second-order scheme at 95% confidence level. Table III shows MLEs and 95% confidence intervals of the parameters. Based on the estimation, we do normality tests on $\hat{\boldsymbol{e}} = (\boldsymbol{I} - \hat{\boldsymbol{B}})^{1/2}(\boldsymbol{x}(\boldsymbol{s}) - \boldsymbol{Z}\hat{\boldsymbol{\gamma}})$ to see whether there is defect in the field. Anderson-Darling test gives a zero p value. Half-normal plot of $\hat{\boldsymbol{e}}$ is also depicted in Fig. 13 to assist the detection. Both indexes strongly indicate the existence of defects. Our method indeed detects defects automatically without observing the images.

Then, we model the NW length field by second order varying coefficient GMRF to identify detailed defect patterns. Model parameters are estimated by the LLE technique. Cross validation

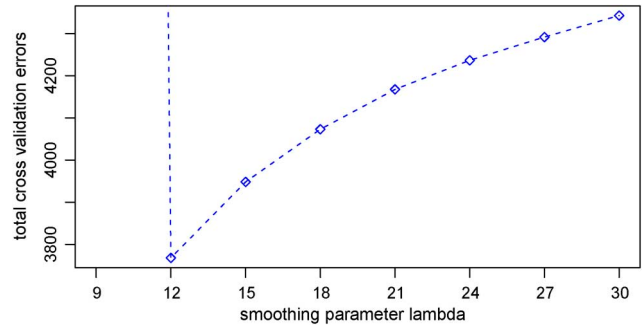

Fig. 14. λ selection by cross validation, real case study.

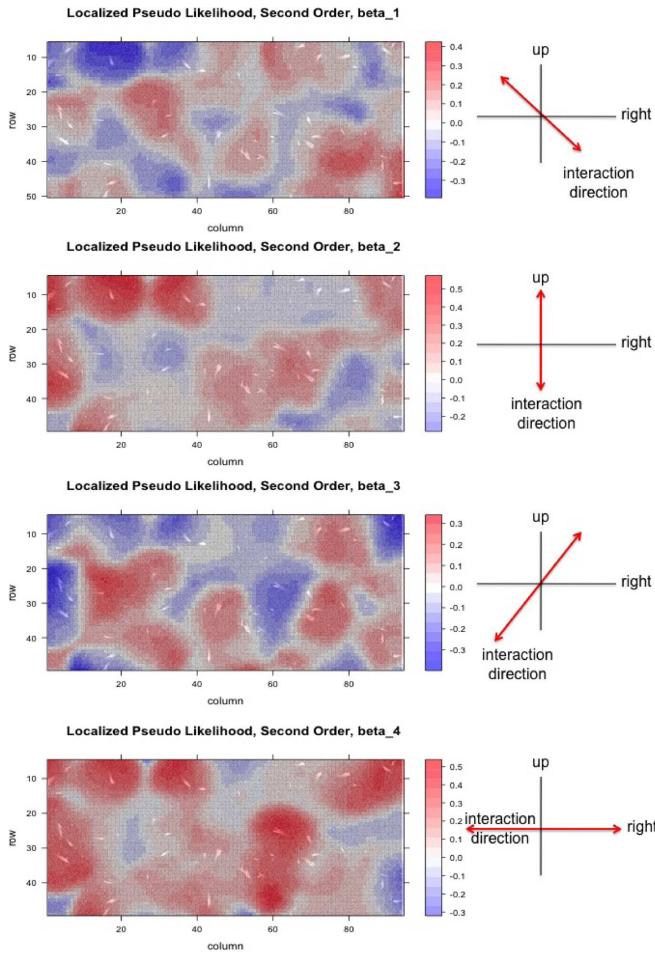

Fig. 15. Level plots of local likelihood estimated $\boldsymbol{\beta}$ together with top view SEM images real case study.

errors under different λ values are shown in Fig. 14. So, $\lambda = 12$ is chosen. We plot estimated $\beta_i, i = 1, \ldots, 4$ across the field on top of the top view SEM image in Fig. 15. As expected, local peaks of interactions always correspond to nanowires bundles. Although length measurements of nanowire bundles are approximate, our extracted patterns of nanowire interactions still identify the patterns of defects satisfactorily.

Nanowire bundles absorb more source materials during the growth process and occupy additional space due to their curved shapes (insets of Fig. 9). As a result, nanowire bundles inhibit the growth of neighboring sites and may even cause no growth

areas around them (Fig. 11). Consequently, their estimated interactions from the length measurement data are stronger than other sites. That is why we may identify defects by "abnormally" strong interactions.

By studying real collected nanowire length data, we can confirm our method to model and estimate nanostructure interactions does automatically detect defects and identify defect patterns. Our studies of nanostructure interactions are consistent with known physical understanding.

Remark 1: Our approach of modeling and estimating nanostructure interactions enables not only the characterization of nanostructure features, but also the detection of defects based on "abnormal" interactions among nanostructures.

Remark 2: Simulation study and real case study show the identification of no growth sites caused by underlying deformities on the substrate and neighboring defective structures (large bundles), respectively. Further research can be done to distinguish these two failure mechanisms.

VII. Summary and Conclusion

In this paper, we develop a technique to model and estimate interactions among neighboring nanostructures for any local region of interest to assist the characterization of local features and automatic diagnosis of structure defects.

We interpret interactions among nanostructures as the mutual contributions on neighbors' feature variability. Under the framework of Gaussian Markov random field, we incorporate nanostructure interactions into the modeling of local features and establish their connections with local feature variability by pairwise conditional correlations. Our strategies of interaction estimation consist of three sequential steps: estimating the stationary interactions by MLE assuming no defects, defect detection by normality tests on transformed residuals based on stationary interaction estimation and estimating the nonstationary interactions by LLE if the region has defects. Estimated interaction patterns identify defect patterns.

Both simulation and real case studies of nanostructure interactions are consistent with existing physical knowledge. Our approach indeed quantifies local feature variability and diagnoses defects accurately and automatically. In addition, our established connection of nanostructure interactions and feature variability will advance both property analysis of nanostructures and physical investigation of structure formation. Further exploration of nanostructure interactions will assist to generate new understandings of process-structure-property relation.

Appendix
Nanowire Length Measurement

Denote $(.)_p$ and $(.)_d$ as location parameters on top view and tilted view images, respectively, where $(.)$ could be Y or α. Let D be the distance between NW tip and the reference point. As illustrated in Fig. 16, we then have the following relations:

$$K = \sqrt{D^2 - X^2} = \frac{Y_p}{\cos(\alpha_p)} = \frac{Y_d}{\cos(\alpha_d)} \tag{A.1}$$

$$Z = \frac{Y_p \sin(\alpha_p)}{\cos(\alpha_p)} \tag{A.2}$$

$$\alpha_p = \alpha_d + \delta \tag{A.3}$$

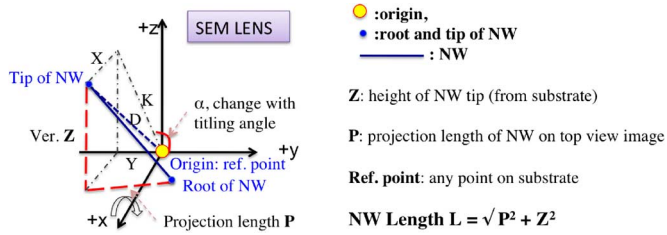

Fig. 16. Geometric model for measuring NW length.

where δ is the known tilting angle which equals 8° in our case. Y_p and Y_d are measurable. Since we tilt around axis x, X and thus K are the same for both images. Therefore, the height of NW tip to the reference point is

$$Z = \frac{Y_p \cos(\delta) - Y_d}{\sin(\delta)}. \tag{A.4}$$

Substituting Z as in (A.4), we obtain the NW length

$$L = \sqrt{P^2 + Z^2} = \sqrt{P^2 + \frac{(Y_p \cos(\delta) - Y_d)^2}{\sin^2(\delta)}} \tag{A.5}$$

where P is the projection length of NW on top view image which is also measurable.

Acknowledgment

The authors would like to thank Dr. C. Zhou's group in University of Southern California for providing ZnO nanowire samples.

References

[1] G. Zheng, F. Patolsky, Y. Cui, W. Wang, and C. Lieber, "Multiplexed electrical detection of cancer markers with nanowire sensor arrays," *Nature Biotechnol.*, vol. 23, no. 10, pp. 1294–1301, 2005.

[2] M. Law, L. Greene, J. Johnson, R. Saykally, and P. Yang, "Nanowire dye-sensitized solar cells," *Nature Materials*, vol. 4, no. 6, pp. 455–459, 2005.

[3] J. Johnson, H. Yan, P. Yang, and R. Saykally, "Optical cavity effects in ZnO nanowire lasers and waveguides," *J. Phys. Chem. B*, vol. 107, no. 34, pp. 8816–8828, 2003.

[4] C. Wang, K. Ryu, L. De Arco, A. Badmaev, J. Zhang, X. Lin, Y. Che, and C. Zhou, "Synthesis and device applications of high-density aligned carbon nanotubes using low-pressure chemical vapor deposition and stacked multiple transfer," *Nano Res.*, vol. 3, no. 12, pp. 831–842, 2010.

[5] C. Wang, K. Ryu, A. Badmaev, J. Zhang, and C. Zhou, "Metal contact engineering and registration-free fabrication of complementary metal-oxide semiconductor integrated circuits using aligned carbon nanotubes," *ACS Nano*, vol. 5, no. 2, pp. 1147–1153, 2011.

[6] E. Garnett and P. Yang, "Light trapping in silicon nanowire solar cells," *Nano Lett.*, vol. 10, no. 3, pp. 1082–1087, 2010.

[7] J. Song, X. Wang, E. Riedo, and Z. L. Wang, "Systematic study on experimental conditions for large-scale growth of aligned ZnO nanowires on nitrides," *J. Phys. Chem.. B*, vol. 109, no. 20, pp. 9869–9872, 2005.

[8] T. Dasgupta, C. Ma, V. Joseph, Z. Wang, and C. Wu, "Statistical modeling and analysis for robust synthesis of nanostructures," *J. Amer. Statist. Assoc.*, vol. 103, no. 482, pp. 594–603, 2008.

[9] Q. Huang, "Physics-driven Bayesian hierarchical modeling of nanowire growth process at each scale," *IIE Trans. Quality Reliability*, vol. 43, pp. 1–11, 2011.

[10] Q. Huang, L. Wang, T. Dasgupta, L. Zhu, P. K. Sekhar, S. Bhansali, and Y. An, "Statistical weight kinetics modeling and estimation for silica nanowire growth catalyzed by pd thin film," *IEEE Trans. Autom. Sci. Eng.*, vol. 8, no. 2, pp. 303–310, Apr. 2011.

[11] T. Dasgupta, B. Weintraub, and V. Joseph, "A physical-statistical model for density control of nanowires," *IIE Trans.*, vol. 43, no. 4, pp. 233–241, 2011.

[12] J. Song, H. Xie, W. Wu, V. R. Joseph, C. J. Wu, and Z. Wang, "Robust optimization of the output voltage of nanogenerators by statistical design of experiments," *Nano Res.*, vol. 3, no. 9, pp. 613–619, 2010.
[13] L. Zhu, T. Dasgupta, and Q. Huang, "A d-optimal design for estimation of parameters of an exponential-linear growth of nanostructures," *Technometrics. Under Review*, 2012.
[14] C. Chang, L. Xu, Q. Huang, and J. Shi, "Quantitative characterization and modeling strategy of nanoparticle dispersion in polymer composites," *IIE Trans.*, vol. 44, no. 7, pp. 523–533, 2012.
[15] L. Zeng, Q. Zhou, M. De Cicco, X. Li, and S. Zhou, "Quantifying boundary effect of nanoparticles in metal matrix nanocomposite fabrication processes," *IIE Trans.*, vol. 44, no. 7, pp. 551–567, 2012.
[16] N. Cressie*, Statistics for Spatial Data*, 2nd ed. New York, US: Wiley, 1993.
[17] J. Besag, "Spatial interaction and the statistical analysis of lattice systems," *J. Royal Statist. Soc., Series B (Methodological)*, vol. 36, no. 2, pp. 192–236, 1974.
[18] R. Mead, "A relationship between individual plant-spacing and yield," *Ann. Botany*, vol. 30, no. 118, pp. 301–309, 1966.
[19] S. Geman and D. Geman, "Stochastic relaxation, Gibbs distributions and the Bayesian restoration of images," *IEEE Trans. Pattern Anal. Mach. Intell.*, vol. 6, pp. 721–741, 1984.
[20] J. Besag, "On the statistical analysis of dirty pictures," *J. Royal Statist. Soc., Series B*, vol. 48, no. 3, pp. 259–302, 1986.
[21] N. Best, K. Ickstadt, R. Wolpert, and D. Briggs*, Combining Models of Health and Exposure Data: The SAVIAH Study*, P. Elliott, J. Wakefield, N. Best, and D. Briggs, Eds. Oxford, U.K.: Oxford Univ. Press, 2000.
[22] D. Brook, "On the distinction between the conditional probability and the joint probability approaches in the specification of nearest-neighbor systems," *Biometrika*, vol. 51, no. 3, pp. 481–483, 1964.
[23] P. Whittle, "On stationary processes in the plane," *Biometrika*, vol. 41, no. 3, pp. 434–449, 1954.
[24] X. Guyon, "Parameter estimation for a stationary process on a d-dimensional lattice," *Biometrika*, vol. 69, no. 1, p. 95, 1982.
[25] J. Besag and P. A. P. Moran, "On the estimation and testing of spatial interaction in Gaussian lattice processes," *Biometrika*, vol. 62, no. 3, pp. 555–562, 1975.
[26] P. Moran, "A Gaussian Markovian process on a square lattice," *J. Appl. Probability*, vol. 10, no. 1, pp. 54–62, 1973.
[27] K. Mardia and R. Marshall, "Maximum likelihood estimation of models for residual covariance in spatial regression," *Biometrika*, vol. 71, no. 1, p. 135, 1984.
[28] H. Thode*, Testing for Normality*. New York: CRC, 2002, vol. 164.
[29] M. Stephens, "EDF statistics for goodness of fit and some comparisons," *J. Amer. Statist. Assoc.*, vol. 69, no. 347, pp. 730–737, 1974.
[30] A. Van der Linde, "On cross-validation for smoothing splines in the case of dependent observations," *Australian & New Zealand J. Statist.*, vol. 36, no. 1, pp. 67–73, 1994.
[31] G. Kauermann and G. Tutz, "Local likelihood estimation in varying-coefficient models including additive bias correction," *J. Nonparametric Statistics*, vol. 12, no. 3, pp. 343–371, 2000.
[32] J. Dreesman and G. Tutz, "Non-stationary conditional models for spatial data based on varying coefficients," *J. Royal Statist. Soc., Series D (The Statistician)*, vol. 50, no. 1, pp. 1–15, 2001.

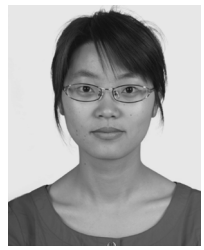

Lijuan Xu received the B.S. degree from the Department of Industrial Engineering, Tsinghua University, Beijing, China, in 2009 and the M.S. degree in statistics from the Department of Mathematics, University of Southern California, Los Angeles, in 2011. She is currently working towards the Ph.D. degree at the Daniel J. Epstein Department of Industrial and Systems Engineering, University of Southern California. Her dissertation research focuses on modeling and estimation of nanostructure spatial interactions for nanomanufacturing quality control.

Her general research interests include modeling, diagnosis and control of advanced manufacuturing systems, applied statistics, and data mining.

Qiang Huang (M'10) is currently an Associate Professor and Gordon S. Marshall Early Career Chair in Engineering in the Daniel J. Epstein Department of Industrial and Systems Engineering, University of Southern California, Los Angeles. Funded by the National Science Foundation (including the CAREER Award) and ONR, his research focuses on modeling and analysis of complex systems for quality and productivity improvement, with special interest in integrated nanomanufacturing and nanoinformatics.

Prof. Huang is a member of the Institute of Industrial Engineers (IIE), the Institute for Operations Research and the Management Sciences (INFORMS), SME, and the American Society of Mechanical Engineers (ASME). He has been an Associate Editor of the IEEE TRANSACTIONS ON AUTOMATION SCIENCE AND ENGINEERING since 2012 and served as Editor (Quality, Micro and Nanomanufacturing Systems) for the *Journal of Manufacturing Systems* from 2008 to 2011. He was one of the editors for the Special Issue of the *IIE Transactions*: Quality, Sensing and Prognostics Issues in Nanomanufacturing. He was a member of the scientific committee (Editorial Board) for the North American Manufacturing Research Institution (NAMRI) of SME, 2009–2011. He was an Associate Editor (*Automation in Meso, Micro and Nano-Scale*) of the 2009 and 2010 IEEE Conferences on Automation Science and Engineering.